Tensor Asymmetry A_{zz} in the $x > 1$ Region

A Proposal to Jefferson Lab PAC 42

E. Long, [†] [‡] K. Slifer,[†] P. Solvignon[†]
University of New Hampshire, Durham, NH 03861

D. Higinbotham[†]
Thomas Jefferson National Accelerator Facility, Newport News, VA 23606

[†]Spokesperson
[‡]Contact: ellie@jlab.org

Abstract

The tensor-polarized target asymmetry, A_{zz}, which is used to extract b_1 in the DIS region through the D(e, e')X channel, can be used to extract information on nucleon-nucleon interactions in the quasi-elastic region. The reaction is unique in that it can probe color transparency, which has never been explored at Jefferson Lab, and improve understanding of the deuteron wave function and particularly probe how short range correlations arise from proton-neutron interactions.

In the quasi-elastic region, A_{zz} was first calculated in 1988 by Frankfurt and Strikman, using the Hamada-Johnstone and Reid soft-core wave functions [1]. Recent calculations by M. Sargsian revisit A_{zz} in the $x > 1$ range using virtual-nucleon and light-cone methods, which differ by up to a factor of two [2].

An experimental determination of A_{zz} could be performed utilizing equipment identical for E13-12-011 at five different Q^2 values over the course of 24 days, with [NUMBER] additional days of commissioning. The measurements are less sensitive to the target polarization than E13-12-011, such that this experiment could be used to prove that the condition of 30% in-beam polarization is met for E13-12-011.

Contents

1 Quotes (To be removed)

1.1 Deuteron Form Factors

"Accurate [form factor] measurements require that Q^2 be known accurately since A and B vary rapidly with Q^2. Energy or angle offsets of a few times 10^{-3} could lead to Q^2 being off by up to 0.5%. For both A and B, this leads to offsets that increase with Q^2, reaching about 2% at $Q^2 = 1$ GeV^2 and 4% at $Q^2 = 6$ GeV^2." -R. Gilman and F. Gross [3]

"The body of [A] data, aside from the lowest Q Orsay point, suggests the correctness of the Saclay measurements. Theoretical predictions span the range between the two data sets, and do not help to determine which is correct. Thus, a new high-precision experiment in this [higher] Q^2 range appears desirable." -R. Gilman and F. Gross [3]

"We are forced to conclude that these high Q^2 [form factor] measurements *cannot be explained by nonrelativistic physics and present very strong evidence for the presence of interaction currents, relativistic effects or possibly new physics*." -R. Gilman and F. Gross [3]

"It is clear that much more work will be needed to clarify the various physics issues, before a convergent scheme is established for treating the e.m. and strong interaction physics properly." -J.A. Tjon [4]

"It turns out that this leading twist pQCD estimate is $10^3 - 10^4$ times smaller than the measured deuteron form factor, implying large soft contributions to the form factor, in agreement with [5, 6], suggesting that pQCD should not be used as an explanation for the form factor. The calculation is extremely complicated and a confirmation, or refutation, is desirable." -R. Gilman and F. Gross [3]

"From the discussions in section 3.8, it is clearly of interest to extend measurements of A to higher Q^2. An ed coincidence experiment is straightforward, but prohibitive timewise with present accelerators. The proposed 12 GeV JLab upgrade allows one to take advantage of the approximate E^2 scaling of σ_M at constant Q^2 and high energy [7]. A large acceptance spectrometer such as MAD would be very helpful. Depending on the details of the upgrade, a one month experiment could provide data to Q^2 of 8 GeV^2." -R. Gilman and F. Gross [3]

1.2 Light Cone Calculations

"It is now known that the tensor part of the one-pion exchange interaction is too strong to be treated pertubatively, and recent work has focused on how to include the singular parts of one-pion exchange in the most effective manner [8, 9, 10]" -R. Gilman and F. Gross [3]

"But a principal motivation for using the front-form is that it is a natural choice at very high momentum, where the interactions single out a preferred direction (the beam direction) and the dynamics evolves along the light-front in that direction. The disadvantage is that the generators that contain dynamical quantities ar H_- and J^i, and this means that angular momentum conservation must be treated as a dynamical constraint." -R. Gilman and F. Gross [3]

"One of the fundamental problems in field theory is the description of the quantum bound states in a relativistically invariant form. The problem inevitably arises with the proper treatment of the time at which the bound state is observed as well as the unambiguous identification of the compositeness of a bound state due to the non-trivial structure of the vacuum in field theories. The

latter is related to the differentiation of the constituents of the bound system from the particles arising from the vacuum fluctuations." -M. Sargsian [11]

1.3 Guides to Experimental Set-Up

"Within the context of a more realistic dynamical theory, one can use response function separations and polarization observables to enhance the sensitivity to various model dependent *unobservables*, such as momentum distributions, meson exchange currents and medium modifications. One strong recent interest has been to choose kinematics in which the unobserved nucleon has a large momentum; the plane wave approximation shows that this configuration enhances sensitivity to initial-state short-range correlations (i.e. the wavefunction) and possibly quark effects. A number of these experiments have been carried out at various accelerators, but no experiments at JLab have yet reported the results." -R. Gilman and F. Gross [3]

"The most precise constraint on these [$I = 1$ exchange] currents comes from the $d \rightarrow^1 S_0$ transition, and this part of the transition is partly obscured by the poor energy resolution of the existing high Q^2 measurements. A new and improved experiment at JLab with higher resolution would allow the threshold $d \rightarrow^1 S_0$ process to be better extracted, with a better resulting determination of the isovector exchange currents. It is also important to determine whether or not there is a minimum near 1.2 GeV^2." -R. Gilman and F. Gross [3]

"Due to the rather small size of this structure, it could have a revealing relation to certain aspects of QCD. Experiments to probe this structure and its effects in nuclei are suggested." -J.L. Forest, et al. [12]

1.4 LiD vs He2D

"From those results, only the ^{6}Li ground state show the LS coupling structure and this can be related to the $\alpha + d$ clustering in the $T = 0$ state. ... The detailed analyses including the excited states are performed in our paper [13]." -T. Myo [14]

1.5 Short Range Correlations

"... there is no clearly correct way to isolate the structure of the nucleon from the structure of the bound state. In model calculations these issues can be handled by separating the problem into two regions: at large separations ($R > R_c$) it is assumed that the system separates into two nucleons interacting through one pion exchange, and at small distances ($R < R_c$) the system is assumed to coalesce into a six-quark bag with all the quarks treated on an equal footing." -R. Gilman and F. Gross [3]

"Calculations based on quark degrees of freedom must confront the fact that the deuteron is at least a six-quark system. Since the six quarks are identical (because of internal symmetries) the system must be antisymmetrized, and it is not clear that the nucleon should retain its identity in the presence of another nucleon." -R. Gilman and F. Gross [3]

"SRCs are considered one of the most elusive features of the ground state nuclear wave functions." -M. Sargsian [15]

"One of the methods in probing 2N SRCs is studying high Q^2 inclusive $A(e,e')X$ scattering at $x > 1.4$ in which case virtual photon scatters off the bound nucleon with momenta exceeding $k_F(A)$ [16, 17]." -M. Sargsian [15]

"However, it is worth noting that there is a growing activity in studies of NN bound systems at short distances by probing the short range correlations in the nuclear wave functions (see e.g. [18, 19, 20, 21, 22]). Currently these studies unambigously identified the tensor component of short-range NN interactions in the nuclear medium. The planned experiments at hte 12 GeV energy upgraded Jefferson Lab [17, 23] will be able to probe the bound NN systems at distances relevant to the nuclear core, where one may expect the onset of QCD degrees of freedom in the similar way as in the hard NN interactions.

"Overall new experiments in studies of both hard NN scattering processes and NN short-range correlations in nuclei will provide the necessary ground for advancing the understanding of QCD dynamics of strong forces at short distances." -M. Sargsian [11]

1.6 Notation and Conventions

"The cross section for the double scattering process can be written as [24]

$$\frac{d\sigma}{d\Omega d\Omega_2} = \left.\frac{d\sigma}{d\Omega d\Omega_2}\right|_0 \left[1 + \frac{3}{2} h p_x A_y \sin\phi_2 + \frac{1}{\sqrt{2}} t_{20} A_{zz} - \frac{2}{\sqrt{3}} t_{21} A_{xz} \cos\phi_2 + \frac{1}{\sqrt{3}} t_{22} \left(A_{xx} - A_{yy}\right) \cos 2\phi_2\right] \tag{1}$$

where $h = \pm 1/2$ is the polarization of the incoming electron beam, ϕ_2 the angle between the two scattering planes (defined in the same way as the ϕ shown in figure 24) and A_y and the A_{ij} are the vector and tensor analysing powers of the second scattering. Although there is a p_z component to the vector polarization, the term is omitted from equation (25) as there is no longitudinal vector analysing power; without spin precession, this term cannot be determined." -R. Gilman and F. Gross [3]

1.7 Tensor Polarization/Force and NN Interactions/SRC

"The most direct evidence for tensor correlations in nuclei comes from measurements of the deuteron structure functions and tensor polarization by elastic electron scattering [3]. In essence, these measurements have mapped out the Fourier transforms of the charge densitites of the deuteron in states with spin projections ± 1 and 0, showing that they are very different." -R. Schiavilla, et al. [25]

"The nucleon-nucleon (NN) interaction has strong tensor forces at long and intermediate distances caused by the pion exchange, which emerges large momentum transfer, and also strong central repulsions at short distance caused by the quark dynamics [26, 27]. It is important to investigate the nuclear structure by treating these characteristics of the NN interaction." -T. Myo [14]

"Another recent news from SRC studies is the observation of a strong (by factor of 20) dominance of pn relative to pp and nn SRC's in the range of the bound nucleon momenta $k_F < p <$

$600\mathrm{MeV}/c$[28, 29]. This observation of was an indication that at the distances relevant to the above momentum range the NN force is dominated by tensor interaction. This gave a new meaning to the above mentioned ratios:

$$A_2(A) = \frac{2 \cdot \sigma_{eA}}{A \cdot \sigma_{ed}}, \tag{2}$$

which now represent (up to the SRC center of mass motion effect) the probability of finding 2N SRCs in the nucleus A. The observed strong disbalance of pn and pp/nn SRCs allowed also to suggest new approximate relation for the high momentum distribution of protons and neutrons in the nucleus A[30]:

$$n^A_{p/n}(p) = \frac{1}{2x_{p/n}} a_d(A, y) \cdot n_d(p) \tag{3}$$

where $x_{p/n} = \frac{Z}{A}/\frac{A-Z}{A}$ and $y = |1 - 2x_p|$." -M. Sargsian [15]

"By decreasing the separation of nucleons to $1.2 - 1.5$ fm one will observe the onset of the strong contribution due to two-pion exchange forces resulting in the tensor interaction. The observed magnitude of the tensor as well as strong spin-orbit interactions, however, requires an addition of the vector component to the exchanged forces whose contribution gradually increases with the decrease of NN separations and dominates the overall interaction in the region of the repulsive core at ≤ 0.5 fm." -M. Sargsian [11]

1.8 6-quark systems, hidden color

"The third aspect which is worth to emphasize in relation to studies of NN interaction at short distances is the dynamics of the NN-bound system probed at short distances. The deuteron studies opened up a new realm in studies of QCD dynamics of strong forces. It was realized in Refs. [31, 32, 33, 34, 35], that the fact, that the deuteron is a colorless 6-valence-quark system, creates an additional possibility for existence of color-octet three-quark (3q) states that combine into color-singlet 6-quark combinations (referred as hidden color states). The calculations indicate that there is a substantial hidden color component in the NN bound system at short distances in which the 6q system becomes a relevant degree of freedom.

"The notion of the hidden-color component gave a new possible meaning to the NN repulsion which can be in part due to orthogonality between the initial two color octet and final two color singlet nucleons. The other implication of the hidden color component is the prediction of the large contribution from the $\Delta - \Delta$ component in the NN interaction following from the decomposition of the color-singlet 6-quark system." -M. Sargsian [11]

"The hidden color component is one of the unique QCD effects in NN interaction that can not be imitated by any baryons degrees of freedom. The hypothesis of the color-neutrality of the observed strongly interacting composite systems introduces the possibilities for a new reality in which baryonic systems with high degree of compositeness (one example is NN system) contain explicitly colored three-quark clusters that combine into a color neutral object. One of the best examples is the contribution of two colored baryons, N_c, into the colorless NN system [31, 33, 34]. While existence of such hidden-color components are accepted within QCD there is no clear experimental evidence yet for such components." -M. Sargsian [11]

1.9 Color transparency

"One of the most remarkable predictions of QCD is the existence of color transparency phenomena in hard processes taking place in the nuclear environment. ... The realization that these small-sized configurations are not eigenstates of QCD Hampiltonian of free hadrons and once produced at finite energies they will evolve to normal size hadrons, suggested that the experimental verification of color transparency phenomena is more complex than first expected (see e.g. Ref. [36, 37].

"While the Color Transparency phenomenon or the reduction of the absorption in the nuclear medium is observed for the hard production of $q\bar{q}$ systems [38, 39, 40], the similar effect is still elusive for a qqq system." -M. Sargsian [11]

1.10 Applications to Astrophysics

"Recent observations of large ($\approx 2M_{Sun}$) neutron star masses [41] indicates existence of rather unreasonably stiff equation of state of the nuclear matter, which is related to the persistence of the nucleonic degrees of freedom [42] at such high densities in which one expects plenty of inelastic transitions and strong overlap of nucleon wave functions. Such persistence is also observed in probing short-range proton-neutron correlations in the nuclei [29, 28] in which the theoretical analysis [18] shows that for up to ≤ 1 fm separations, the NN system has no apparent non-nucleonic component, consisting almost entirely from proton and neutron.

"It is interesting that this observation also has its reflection in the modification of partonic distributions of bound nucleons in the nuclear medium (EMC effect). Here, the recent analysis [43] indicates a rather small modification of nucleons in the medium of heavy nuclei, which seems puzzling.

"Such a persistence of the nucleons in the high density nuclear environment can be due to the short range repulsion, since the attractive interaction will make the composite system very responsive to medium modifications." -M. Sargsian [11]

2 Background and Motivation

The deuteron is the simplest composite nuclear system, and in many ways it is as important to understanding bound states in QCD as the hydrogen atom was to understanding bound systems in QED. Our experimental and theoretical understanding of the deuteron remains unsatisfying. By taking a ratio of electron scattering off of tensor-polarized and unpolarized deuterons, the S- and D-wave states can be disentangled, leading to a fuller understanding of the repulsive nucleon core.

Understanding the nucleon-nucleon potential of the deuteron is essential for understanding short-range correlations. To resolve the short-range structure of nuclei on the level of nucleon and hadronic constituents, we need processes that transfer to the nucleon constituents both energy and momentum larger than the scale of the NN short range correlations. By scanning over a large range of Q^2, we can measure how these processes begin to dominate the tensor asymmetry A_{zz}.

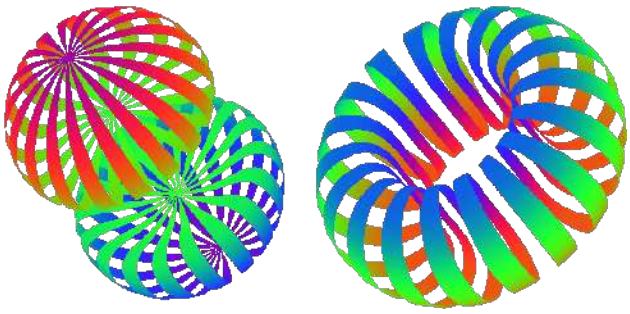

Figure 1: Equidensity lines of the deuteron in its two spin projections, $M_J = \pm 1$ and $M_J = 0$, respectively. *Reproduced from [45, 12].*

2.1 Deuteron Wavefunction

2.2 Tensor Asymmetry Azz

The S- and D-states are to the tensor asymmetry A_{zz} by [1]

$$A_{zz} \propto \frac{u(k)w(k)\sqrt{2} + \frac{1}{2}w^2(k)}{u^2(k) + w^2(k)}, \tag{4}$$

where $u(k)$ is the ${}^3S_1$ wave function and $w(k)$ is the ${}^3D_1$ wave function.

For decades [44], it has been known that the nucleon-nucleon potential has a short-range repulsive core, which is responsible for the stability of strongly interacting matter. However, a description of the repulsive core remains largely unconstrained and our understanding of QCD dynamics at short distances (≤ 0.5 fm) largely incomplete [11].

Due to their small size [**?**] and simple structure, tensor polarized deuterons are ideal for studying nucleon-nucleon interactions. Tensor polarization enhances the D-state wavefunction, which compresses the deuteron from $\sim ?$ fm to $\sim$ 0.5 fm [12] and has been noted to be revealing of short-range QCD effects.

3 The Proposed Experiment

3.1 Experimental Method

As in the case for E12-13-011, the measured double differential cross section for a spin-1 target characterized by a vector polarization P_z and tensor polarization P_{zz} is expressed as,

$$\frac{d^2\sigma_p}{d\Omega dE'} = \frac{d^2\sigma_u}{d\Omega dE'}\left(1 - P_z P_B A_1 + \frac{1}{2}P_{zz}A_{zz}\right), \tag{5}$$

where, σ_p (σ_u) is the polarized (unpolarized) cross section, P_B is the incident electron beam polarization, and A_1 (A_{zz}) is the vector (tensor) asymmetry of the virtual-photon deuteron cross section.

This allows us to write the polarized tensor asymmetry with $0 < P_{zz} \leq 1$ using an unpolarized electron beam as

$$A_{zz} = \frac{2}{P_{zz}} \left(\frac{\sigma_p - \sigma_u}{\sigma_u} \right), \tag{6}$$

where σ_p is the polarized cross section. The tensor polarization is given by

$$P_{zz} = \frac{n_+ - 2n_0 + n_-}{n_+ + n_- + n_0}, \tag{7}$$

where n_m represents the population in the $m_z = +1$, -1, or 0 state.

Eq. 6 reveals that the asymmetry A_{zz} compares two different cross sections measured under different polarization conditions of the target: positively tensor polarized and unpolarized. To obtain the relative cross section measurement in the same configuration, the same target cup and material will be used at alternating polarization states (polarized vs. unpolarized), and the magnetic field providing the quantization axis will be oriented along the beamline at all times. This field will always be held at the same value, regardless of the target material polarization state. This process, identical to that used for the E12-13-011 b_1 measurement, ensures that the acceptance remains consistent within the stability (10^{-4}) of the super conducting magnet.

Since many of the factors involved in the cross sections cancel in the ratio, Eq. 6 can be expressed in terms of the charge normalized, efficiency corrected numbers of tensor polarized (N_p) and unpolarized (N_u) counts,

$$A_{zz} \;\; = \;\; \frac{2}{f P_{zz}} \left(\frac{N_p - N_u}{N_u} \right). \tag{8}$$

The dilution factor f corrects for the presence of unpolarized nuclei in the target and is defined by

$$f = \frac{N_D \sigma_D}{N_N \sigma_N + N_D \sigma_D + \sum\limits_A N_A \sigma_A}, \tag{9}$$

where N_D is the number of deuterium nuclei in the target and σ_D is the corresponding inclusive double differential scattering cross section, N_N is the nitrogen number of scattered nuclei with cross section σ_N, and N_A is the number of other scattering nuclei of mass number A with cross section σ_A. As has been noted in previous work [1], the dilution factor at high x drops off considerably until the SRC plateau region, as shown in Fig. 2. By using a high-luminosity solid target and a low angle $\theta_{e'}$, this effect will be largely counteracted.

The dilution factor can be written in terms of the relative volume ratio of ND_3 to LHe in the target cell, otherwise known as the packing fraction p_f. In our case of a cylindrical target cell oriented along the magnetic field,the packing fraction is exactly equivalent to the percentage of the cell length filled with ND_3.

If the time is evenly split between scattering off of polarized and unpolarized ND_3, the time necessary to achieve the desired precision δA is:

$$T = \frac{N_p}{R_p} + \frac{N_u}{R_u} = \frac{8}{f^2 P_{zz}^2} \left(\frac{R_p (R_u + R_p)}{R_u^3} \right) \frac{1}{\delta A_{zz}^2} \tag{10}$$

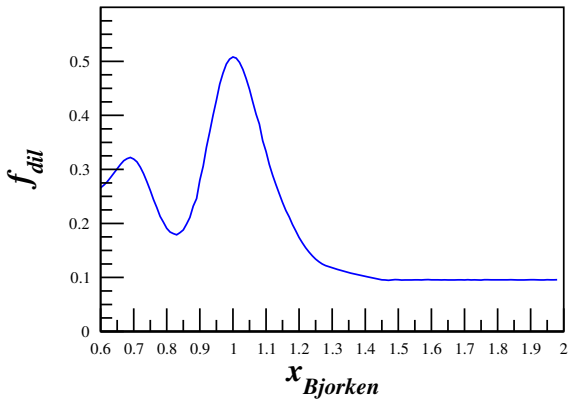

Figure 2: The estimated dilution factor, in this case at $Q^2 = 1.5\ (\mathrm{GeV}/c)^2$, is expected to drop off at high x until it reaches the SRC plateau region. This effect will be counteracted by using a high-luminosity solid target.

where $R_{p(u)}$ is the polarized (unpolarized) rate and $N_{p(u)}$ is the total estimated number of polarized (unpolarized) counts to achieve the uncertainty δA_{zz}.

3.1.1 Statistical Uncertainty

To investigate the statistical uncertainty we start with the equation for A_{zz} using measured counts for polarized data (N_p) and unpolarized data (N_u),

$$A_{zz} = \frac{2}{f P_{zz}} \left(\frac{N_p}{N_u} - 1 \right). \tag{11}$$

The statistical error with respect to counts is then

$$\delta A_{zz} = \frac{2}{f P_{zz}} \sqrt{\left(\frac{\delta N_p}{N_u} \right)^2 + \left(\frac{N_p \delta N_u}{N_u^2} \right)^2}. \tag{12}$$

3.1.2 Systematic Uncertainty

Table 1 shows a list of the scale dependent uncertainties contributing to the systematic error in A_{zz}.

With careful minimization, the uncertainty in P_z can be held to better than 4%, as demonstrated in the recent g2p/GEp experiment [46]. This leads to a a relative uncertainty in P_{zz} of 7.7%. Alternatively, the tensor asymmetry can be directly extracted from the NMR lineshape as discussed in Sec. 3.2, with similar uncertainty. The uncertainty from the dilution factor and packing fraction of the ammonia target contributes at the 4% level. The systematic effect on A_{zz} due to the QED radiative corrections will be quite small. For our measurement there will be no polarized radiative corrections at the lepton vertex, and the unpolarized corrections are known to better than 1.5%.

Charge calibration and detector efficiencies are expected to be known better to 1%, but the impact of time-dependent drifts in these quantities must be carefully controlled.

Source	Systematic
Polarimetry	7.7%
Dilution/packing fraction	4.0%
Radiative corrections	1.5%
Charge Determination	1.0%
Detector resolution and efficiency	1.0%
Total	10%

Table 1: Estimates of the scale dependent contributions to the systematic error of A_{zz}.

Time dependent factors

Eq. 8 involves the ratio of counts, which leads to cancellation of several first order systematic effects. However, the fact that the two data sets will not be taken simultaneously leads to a sensitivity to time dependent variations which will need to be carefully monitored and suppressed. To investigate the systematic differences in the time dependent components of the ntegrated counts, we need to consider the effects from calibration, efficiency, acceptance, and luminosity between the two polarization states.

Fluctuations in luminosity due to target density variation can easily be kept to a minimum by keeping the material beads at the same temperature for both polarization states by control of the microwave and the LHe evaporation. The He vapor pressure reading can give accuracy of material temperature changes at the level of $\sim$0.1%. Beam rastering can also be controlled to a high degree.

The acceptance of each cup can only change as a function of time if the magnetic field changes. The capacity to set, reset, and hold the target superconducting magnet to a desired holding field causes a field uncertainty of only $\delta B/B = 0.01\%$. This implies that, like the cup length l, the acceptance $\mathcal{A}$ for each polarization state is the same.

In order to look at the effect on A_{zz} due to drifts in beam current monitor calibration and detector efficiency, we rewrite Eq. 8 explicitly in terms of the raw measured counts N_p^c and N_u^c,

$$\begin{aligned} A_{zz} &= \frac{2}{fP_{zz}}\left(\frac{N_p^c}{N_u^c} - 1\right) \\ &= \frac{2}{fP_{zz}}\left(\frac{Q\varepsilon l\mathcal{A}}{Q_1\varepsilon_1 l\mathcal{A}}\frac{N_p}{N_u} - 1\right) \end{aligned} \tag{13}$$

where Q represents the accumulated charge, and ε is the detector efficiency. The target length l and acceptance $\mathcal{A}$ are identical in both states to first order.

We can then express Q_1 as the change in beam current measurement calibration that occurs in the time it takes to collect data in one polarization state before switching to another, such that $Q_1 = Q(1 - dQ)$. In this notation dQ is a dimensionless ratio of changes in different polarization states. A similar representation is used for drifts in detector efficiency leading to,

$$A_{zz} = \frac{2}{fP_{zz}}\left(\frac{N_pQ(1-dQ)\varepsilon(1-d\varepsilon)}{N_uQ\varepsilon} - 1\right). \tag{14}$$

which simplifies to,

$$A_{zz} = \frac{2}{fP_{zz}} \left(\frac{N_p}{N_u}(1 - dQ - d\varepsilon + dQd\varepsilon) - 1 \right). \tag{15}$$

For estimates of the dQ and $d\varepsilon$ we turn to previous experimental studies. For HRS detector drift during the JLab transversity experiment E06-010, the detector response was measured such that the normalized yield for same condition over a three month period indicated little change ($< 1\%$). These measurement were then used to show that for short time (20 minutes periods between target spin flip), the detector drift was estimated to be less than 1% times the ratio of the time period between target spin flip and three months. For the present experiment we use the same estimate except for the period between target polarization states used is $\sim$12 hours leading to an overall drift $d\varepsilon \sim 0.01\%$. A similar approach can be used to establish an estimate for dQ using studies from the data from the (g2p/GEp) experiment resulting in $d\varepsilon \sim 0.01\%$.

To express A_{zz} in terms of the estimated experimental drifts in efficiency and current measurement we can write,

$$A_{zz} = \frac{2}{fP_{zz}} \left(\frac{N_1}{N} - 1 \right) \pm \frac{2}{fP_{zz}} d\xi. \tag{16}$$

This leads to a contribution to A_{zz} on the order of 1×10^{-3},

$$dA_{zz}^{drift} = \pm \frac{2}{fP_{zz}} d\xi = \pm 3.7 \times 10^{-3}. \tag{17}$$

Though a very important contribution to the error this value allows a clean measurement of $A_{zz} = 0$ at $x = 0.45$ without overlap with the Hermes error bar. For this estimate we assume only two polarization state changes in a day. If it is possible to increase this rate then the systematic effect in A_{zz} will decrease accordingly.

Naturally detector efficiency can drift for a variety of reasons, for example including fluctuations in gas quality, HV drift or drifts in the spectrometers magnetic field. All of these types of variation as can be realized both during the experiment though monitoring as well as systematic studies of the data collected.

It can be difficult to know changes in luminosity, however the identical condition of the two polarization states minimizes the relative changes in time. There are also checks on the consistency of the cross section data that can be use ensuring the quality of each run used in the asymmetry analysis. Each of these systematic effects can mitigate the systematic uncertainty to ~ 0.001, which is required for the b_1 measurement. In the kinematic region proposed here, A_{zz} is expected to be much larger, on the order of 0.1 to 1.0. While typical false asymmetries in Hall C of 0.01 are acceptable for this proposed measurement, it can also allow for a test of the methods used to reduce them further.

We will measure the tensor asymmetry $A_{zz}$for $0.80 < x < 1.75$, 1.0 (GeV/c)^2 $< Q^2 <$ 1.9 (GeV/c)^2 and $0.59 < W < 1.09$ GeV. Fig. 3 shows the planned kinematic coverage utilizing the Hall C HMS and SHMS spectrometers at forward angle.

The polarized ND_3 target is discussed in section 3.2. The magnetic field of the target will be held constant along the beamline at all times, while the target state is alternated between a polarized and unpolarized state. The tensor polarization and packing fraction used in the rates estimate are

	E_0 (GeV)	$\overline{Q^2}$ (GeV^2)	$\overline{W}$ (GeV)	P_0 (GeV)	θ (deg.)	Rates (kHz)	PAC Time (hours)
SHMS	8.8	1.5	0.46	8.36	8.2	0.55	600
SHMS	6.6	0.7	0.60	6.50	8.2	4.08	90
SHMS	2.2	0.3	0.87	2.11	14.4	3.73	30
HMS	2.2	0.3	0.86	2.11	14.9	4.65	30

Table 2: Summary of the kinematics and physics rates using the Hall C spectrometers.

$\overline{x}$	$\overline{Q^2}$ (GeV^2)	$\overline{W}$ (GeV)	f_{dil}	δA_{zz}^{stat} $\times 10^{-2}$
0.80	1.30	1.09	0.177	0.62
0.90	1.30	1.01	0.293	0.37
1.00	1.30	0.94	0.512	0.20
1.10	1.30	0.88	0.346	0.41
1.20	1.30	0.83	0.180	1.10
1.30	1.30	0.78	0.108	2.38
1.40	1.30	0.73	0.071	4.74
1.55	1.30	0.67	0.046	7.02
1.75	1.30	0.59	0.034	13.8

Table 3: Summary of the expected statistical uncertainty after combining overlapping x-bins. Values represent the statistics weighted average of all events that satisfy our kinematic cuts.

Figure 3: Kinematic coverage. The grey settings are not included in our rates estimates since they fall outside of $0.80 < x < 1.75$. The highlighted represent the central value of the spectrometer setting, which are not the statistics weighted average of the distribution. The shading represents areas with greater statistics.

Figure 4: Projected dilution fraction covering the entire x range to be measured using the Bosted fits [47] for the SHMS and HMS. In the kinematics used, both dilution factors overlap.

Figure 5: Projected statistical errors for the tensor asymmetry A_{zz} with 30 days of beam time. Data at different Q^2 are combined with an x-binning that varies slightly per point, but is approximately ± 0.05. The band represents the systematic uncertainty. Also shown are the calculations from Frankfurt and Strikman [1].

30% and 0.65 , respectively. The packing fraction changes with x in the range of this measurement as shown in Fig. 4. With an incident electron beam current of 115 nA, the expected deuteron luminosity is 1.57×10^{35} / cm^2·s^1. The momentum bite and the acceptance were assumed to be $\Delta P = \pm 8\%$ and $\Delta\Omega = 5.6$ msr for the HMS, and $\Delta P = ^{+20\%}_{-8\%}$ and $\Delta\Omega = 4.4$ msr for the SHMS. For the choice of the kinematics, special attention was taken onto the angular and momentum limits of the spectrometers: for the HMS, $10.5^\circ \leq \theta \leq 85^\circ$ and $1 \leq P_0 \leq 7.3$ GeV/c, and for the SHMS, $5.5^\circ \leq \theta \leq 40^\circ$ and $2 \leq P_0 \leq 11$ GeV/c. In addition, the opening angle between the spectrometers is physically constrained to be larger than 17.5°. The invariant mass W was kept to $W \geq 0.59$ GeV for all settings. The projected uncertainties and A_{zz} are summarized in Table 3, and displayed in Fig. 5.

A total of 30 days of beam time is requested for production data, with an additional 5 days of expected overhead.

Figure 6: Cross section view of the JLab/UVa polarized target. Figure courtesy of C. Keith.

Figure 7: **Top**: NMR signal for ND_3 with a vector polarization of approximately 50% from the GEN experiment. **Bottom**: Relationship between vector and tensor polarization in equilibrium, and neglecting the small quadrupole interaction.

3.2 Polarized Target

This experiment will use the JLab/UVa dynamically polarized solid ND_3 target operated in longitudinal mode. The target is typically operated with a specialized slow raster, and beamline instrumentation capable of characterizing the low current 50-100 nA beam. All of these requirements have been met previously in Hall C. The polarized target (see Fig. 6), has been successfully used in experiments E143, E155, and E155x at SLAC, and E93-026, E01-006 and E07-003, E08-027 and E08-007 at JLab. A similar target was used in Hall B for the EG1,EG4 and DVCS experiments.

The JLAb/UVa target underwent significant renovation and improvement [48] during the recent g2p run. The magnet was replaced early in the run, and the target then performed consistently at or above historical levels. A new 1 K refrigerator and target insert were designed and constructed by the JLab target group. The cryogenic pumping system has been overhauled. In particular, the older Alcatel 2060H rotary vane pumps have been replaced with new Pfeiffer DU065 magnetically coupled rotary vane pumps, and the pump controls are being refurbished. The target motion system has been rebuilt from scratch.

The target operates on the principle of Dynamic Nuclear Polarization, to enhance the low temperature (1 K), high magnetic field (5 T) polarization of solid materials by microwave pumping. The polarized target assembly contains several target cells of 3.0 cm length that can be selected individually by remote control to be located in the uniform field region of a superconducting Helmholtz pair. The permeable target cells are immersed in a vessel filled with liquid Helium and maintained at 1 K by use of a high power evaporation refrigerator. The coils have a 50° conical shaped aperture along the beam axis which allow for unobstructed forward scattering.

The target material is exposed to microwaves to drive the hyperfine transition which aligns the nucleon spins. The heating of the target by the beam causes a drop of a few percent in the polarization, and the polarization slowly decreases with time due to radiation damage. Most of the radiation damage can be repaired by periodically annealing the target, until the accumulated dose reached is greater than about 0.5×10^{17} e^-/cm^2, at which time the target material needs to be replaced.

3.2.1 Polarization Analysis

The three Zeeman sublevels of the deuteron system ($m = -1, 0, 1$) are shifted unevenly due to the quadrupole interaction [49]. This shift depends on the angle between the magnetic field and

Figure 8: Performance of the ND_3 target during the GEN experiment.

the electrical field gradient, and gives rise to two separate transition energies. Hence, the unique double peaked response displayed in Fig. 7. When the system is at thermal equilibrium with the solid lattice, the deuteron polarization is known from:

$$P_z = \frac{4 + \tanh \frac{\mu B}{2kT}}{3 + \tanh^2 \frac{\mu B}{2kT}} \tag{18}$$

where μ is the magnetic moment, and k is Boltzmann's constant. The vector polarization can be determined by comparing the enhanced signal with that of the TE signal (which has known polarization). This polarimetry method is typically reliable to about 5% relative.

Similarly, the tensor polarization is given by:

$$P_{zz} = \frac{4 + \tanh^2 \frac{\mu B}{2kT}}{3 + \tanh^2 \frac{\mu B}{2kT}} \tag{19}$$

From Eqs. 18 and 19, we find:

$$P_{zz} = 2 - \sqrt{4 - 3P_z^2}$$

In addition to the TE method, polarizations can be determined by analyzing NMR lineshapes as described in [50] with a typical 7% relative uncertainty. At high polarizations, the intensities of the two transitions differ, and the NMR signal shows an asymmetry R in the value of the two peaks, as shown in Fig. 7. The vector polarization is then given by:

$$P_z = \frac{R^2 - 1}{R^2 + R + 1} \tag{20}$$

and the tensor polarization is given by:

$$P_{zz} = \frac{R^2 - 2R + 1}{R^2 + R + 1} \tag{21}$$

The DNP technique produces deuteron vector polarizations of up to 60% in ND_3 and 64% in LiD [51], which corresponds to tensor polarizations of approximately 30%. The target polarization decays while in beam, so that the average vector polarization was about 35% in the GEN experiment, as seen if Fig. 8.

An average tensor polarization of 30% enables a significant measurement of $b_1(x)$, as shown in Fig. 5. Any improvement to the expected polarization, although not strictly necessary, would allow the addition of kinematic points, and/or improved statistical accuracy. With this in mind, we are pursuing techniques to enhance the tensor polarization by directly stimulating transitions to/from the $M_s = 0$ state, as discussed in Ref. [49]. D. Crabb from the UVa group had some success in obtaining enhanced tensor polarizations via RF saturation of one of the Zeeman transitions, otherwise known as "hole-burning". The method was not pursued due to the lack of need for tensor polarized targets at the time of the study. Another method to enhance tensor polarization entails simultaneously pumping the sample with two independent microwave frequencies, which requires careful isolation of the respective cavities.

3.2.2 Depolarizing the Target

To move from polarized to unpolarized measurements, the target polarization will be annihilated using destructive NMR loop field changes and destructive DNP microwave pumping. It is also possible to remove LHe in the nose of the target to remove the polarization by heating. During unpolarized data taking the incident electron beam heating is enough to remove the thermal equilibrium polarization.

The NMR measurement will ensure zero polarization. The target material will be kept at $\sim$1 K for polarized and unpolarized data collection, and the target field will be held constant for both states as well. These consistencies are used to minimize the systematic differences in the polarized and unpolarized data collection. To minimize systematic effects over time, the polarization condition will be switched twice in a 24 hour period. This is expected to account for drift in integrated charge accumulation.

3.2.3 Rendering Dilution Factor

To derive the dilution factor, we first start with the ratio of polarized to unpolarized counts. In each case, the number of counts that are actually measured, neglecting the small contributions of the thin aluminium cup window materials, NMR coils, etc., are

$$N_1 = Q_1 \varepsilon_1 \mathcal{A}_1 l_1 [(\sigma_N + 3\sigma_1) p_f + \sigma_{He}(1 - p_f)], \tag{22}$$

and

$$N = Q \varepsilon \mathcal{A} l [(\sigma_N + 3\sigma) p_f + \sigma_{He}(1 - p_f)]. \tag{23}$$

where Q represents accumulated charge, ε is the dectector efficiency, $\mathcal{A}$ the cup acceptance, and l the cup length.

For this calculation we assume similar charge accumulation such that $Q \simeq Q_1$, and that the efficiencies stay constant, in which case all factors drop out of the ratio leading to

$$\begin{aligned}
\frac{N_1}{N} &= \frac{(\sigma_N + 3\sigma_1) p_f + \sigma_{He}(1 - p_f)}{(\sigma_N + 3\sigma) p_f + \sigma_{He}(1 - p_f)} \\
&= \frac{(\sigma_N + 3\sigma(1 + A_{zz} P_{zz}/2)) p_f + \sigma_{He}(1 - p_f)}{(\sigma_N + 3\sigma) p_f + \sigma_{He}(1 - p_f)} \\
&= \frac{[(\sigma_N + 3\sigma) p_f + \sigma_{He}(1 - p_f)] + 3\sigma A_{zz} P_{zz}/2}{(\sigma_N + 3\sigma) p_f + \sigma_{He}(1 - p_f)} \\
&= 1 + \frac{3\sigma A_{zz} P_{zz}/2}{(\sigma_N + 3\sigma) p_f + \sigma_{He}(1 - p_f)} \\
&= 1 + \frac{1}{2} f A_{zz} P_{zz},
\end{aligned} \tag{24}$$

where $\sigma_1 = \sigma(1 + A_{zz} P_{zz}/2)$ has ben substituted, per Eq. 5, with $P_B = 0$. It can be seen that the above result corresponds to Eq. 8.

References

[1] L. Frankfurt and M. Strikman, Phys.Rept. **160**, 235 (1988).

[2] M. Sargsian, private communication, to be published.

[3] R. A. Gilman and F. Gross, J.Phys. **G28**, R37 (2002).

[4] J. A. Tjon, AIP Conference Proceedings **334**, 177 (1995).

[5] N. Isgur and C. Llewellyn Smith, Nucl.Phys. **B317**, 526 (1989).

[6] A. Radyushkin, Nucl.Phys. **A532**, 141 (1991).

[7] G. Petratos, AIP Conf.Proc. **549**, 438 (2000).

[8] D. R. Phillips, G. Rupak, and M. J. Savage, Phys.Lett. **B473**, 209 (2000).

[9] D. R. Phillips and T. Cohen, Nucl.Phys. **A668**, 45 (2000).

[10] M. Walzl and U. G. Meissner, Phys.Lett. **B513**, 37 (2001).

[11] M. M. Sargsian, (2014).

[12] J. L. Forest *et al.*, Phys. Rev. **C54**, 646 (1996).

[13] T. Myo, A. Umeya, H. Toki, and K. Ikeda, Phys.Rev. **C86**, 024318 (2012).

[14] T. Myo, Few Body Syst. **54**, 849 (2013).

[15] M. M. Sargsian, (2012).

[16] M. M. Sargsian, Int.J.Mod.Phys. **E10**, 405 (2001).

[17] M. Sargsian, J. Arrington, W. Bertozzi, W. Boeglin, C. Carlson, *et al.*, J.Phys. **G29**, R1 (2003).

[18] L. Frankfurt, M. Sargsian, and M. Strikman, Int.J.Mod.Phys. **A23**, 2991 (2008).

[19] L. Frankfurt, M. Strikman, D. Day, and M. Sargsian, Phys.Rev. **C48**, 2451 (1993).

[20] J. Arrington, D. Higinbotham, G. Rosner, and M. Sargsian, Prog.Part.Nucl.Phys. **67**, 898 (2012).

[21] M. M. Sargsian, Phys.Rev. **C82**, 014612 (2010).

[22] W. Boeglin *et al.*, Phys.Rev.Lett. **107**, 262501 (2011).

[23] T. J. N. A. F. (U.S.), *The Science Driving the 12 GeV Upgrade of CEBAF.* (Jefferson Lab, ADDRESS, 2000).

[24] R. Arnold, C. E. Carlson, and F. Gross, Phys.Rev. **C21**, 1426 (1980).

[25] R. Schiavilla, R. B. Wiringa, S. C. Pieper, and J. Carlson, Phys.Rev.Lett. **98**, 132501 (2007).

[26] S. C. Pieper and R. B. Wiringa, Ann.Rev.Nucl.Part.Sci. **51**, 53 (2001).

[27] H. Kamada, A. Nogga, W. Gloeckle, E. Hiyama, M. Kamimura, *et al.*, Phys.Rev. **C64**, 044001 (2001).

[28] E. Piasetzky, M. Sargsian, L. Frankfurt, M. Strikman, and J. Watson, Phys.Rev.Lett. **97**, 162504 (2006).

[29] R. Subedi, R. Shneor, P. Monaghan, B. Anderson, K. Aniol, *et al.*, Science **320**, 1476 (2008).

[30] M. McGauley and M. M. Sargsian, (2011).

[31] M. Harvey, Nucl.Phys. **A352**, 326 (1981).

[32] I. Obukhovsky, Y. Smirnov, and Y. Chuvilsky, J.Phys. **A15**, 7 (1982).

[33] S. J. Brodsky and C.-R. Ji, Phys.Rev. **D33**, 1951 (1986).

[34] C.-R. Ji and S. J. Brodsky, Phys.Rev. **D34**, 1460 (1986).

[35] A. Kusainov, V. Neudatchin, and I. Obukhovsky, Phys.Rev. **C44**, 2343 (1991).

[36] G. Farrar, H. Liu, L. Frankfurt, and M. Strikman, Phys.Rev.Lett. **61**, 686 (1988).

[37] B. Kopeliovich, J. Nemchik, and I. Schmidt, Phys.Rev. **C76**, 015205 (2007).

[38] L. Frankfurt, G. Miller, and M. Strikman, Phys.Lett. **B304**, 1 (1993).

[39] L. El Fassi, L. Zana, K. Hafidi, M. Holtrop, B. Mustapha, *et al.*, Phys.Lett. **B712**, 326 (2012).

[40] B. Clasie, X. Qian, J. Arrington, R. Asaturyan, F. Benmokhtar, *et al.*, Phys.Rev.Lett. **99**, 242502 (2007).

[41] P. Demorest, T. Pennucci, S. Ransom, M. Roberts, and J. Hessels, Nature **467**, 1081 (2010).

[42] H. Heiselberg and V. Pandharipande, Ann.Rev.Nucl.Part.Sci. **50**, 481 (2000).

[43] L. Frankfurt and M. Strikman, Int.J.Mod.Phys. **E21**, 1230002 (2012).

[44] R. Jastrow, Phys. Rev. **81**, 165 (1951).

[45] J. Carlson and R. Schiavilla, Rev. Mod. Phys. **70**, 743 (1998).

[46] D. Keller, "Uncertainty in DNP Target Data for E08-007", JLab-TN-12-051.

[47] P. Bosted and V. Mamyan, (2012).

[48] C. Keith, JLab polarized target group. Private communication.

[49] W. Meyer *et al.*, Nucl. Instrum. Meth. **A244**, 574 (1986).

[50] C. Dulya *et al.*, Nucl. Instrum. Meth. **A398**, 109 (1997).

[51] S. L. Bueltmann *et al.*, Nucl. Instrum. Meth. **A425**, 23 (1999).